Published in final edited form as:
Cancer Res. 2014 November 15; 74(22): 6452–6462. doi:10.1158/0008-5472.CAN-14-1408.

Host deficiency in caveolin-2 inhibits lung carcinoma tumor growth by impairing tumor angiogenesis

Yajun Liu, **Sungchan Jang**, **Leike Xie**, and **Grzegorz Sowa***
Department of Medical Pharmacology and Physiology, University of Missouri, Columbia, MO 65212

Abstract

Caveolin-2 (Cav-2), a member of caveolin protein family is largely different from better known caveolin-1 (Cav-1) and thus might play distinct functions. Here, we provide the first genetic evidence suggesting that host-expressed Cav-2 promotes subcutaneous tumor growth and tumor-induced neovascularization using two independent syngeneic mouse models. Host deficiency in Cav-2 resulted in defective and reduced growth of subcutaneously implanted Lewis lung carcinoma (LLC) and B16-F10 melanoma tumors, respectively. Consistent with the defective growth, LLC and B16-F10 melanoma tumors implanted into Cav-2 KO mice displayed reduced microvascular density (MVD) determined by immunohistochemistry with anti-CD31 antibodies, suggesting impaired pathological angiogenesis. Additional studies involving LLC tumors extracted from Cav-2 KO mice just 10 days after implantation determined reduced cell proliferation, massive necrotic cell death and fibrosis. In contrast to day 10, only MVD but not cell proliferation and survival was reduced in the earliest palpable LLC tumors extracted 6 days after implantation into Cav-2 KO mice, suggesting that impaired angiogenesis is the causative factor. Mechanistically, impaired LLC tumor growth and angiogenesis in Cav-2 KO mice was associated with increased expression levels of anti-angiogenic thrombospondin-1 and inhibited S1177 phosphorylation of endothelial nitric oxide synthase. Taken together, our data suggest that host deficiency in Cav-2 impairs tumor-induced angiogenesis, leading to compromised tumor cell survival/proliferation manifested by the defective tumor growth. In conclusion, host-expressed Cav-2 may promote tumor growth via supporting tumor-induced angiogenesis. Thus Cav-2 expressed in tumor microenvironment may potentially become a novel target for cancer therapy.

Keywords

Caveolin-2; Cancer; tumor growth; tumor angiogenesis; Lewis lung carcinoma; B16 melanoma; Thrombospondin-1

*To whom correspondence should be addressed: Grzegorz Sowa, Department of Medical Pharmacology and Physiology, University of Missouri, 1 Hospital Drive, Rm. MA 415, Columbia, MO 65212, Tel. (573) 884-3188; Fax. (573) 884-4276; (sowag@health.missouri.edu). .

Disclosure of Potential Conflict of Interest: No potential conflict of interest is disclosed

Introduction

Caveolins are key components of detergent resistant cholesterol lipid rich membranes including lipid rafts and caveolae. Caveolin-1 (Cav-1) and -2 are ubiquitously expressed and interact with each other, while Cav-3 is muscle specific (1). Despite similar name, the amino acid sequence between Cav-1 and Cav-2 is only 38% identical (62% different) (2), suggesting distinct functional roles for each of these proteins (Reviewed by (3)). However, in contrast to extensively studied Cav-1, much less is known about Cav-2. Nevertheless, most recent studies suggest that Cav-2 could be involved in regulating various processes and functions, in particular in endothelial cells and other cell types (3-12).

In order to grow beyond ca. 2 mm^3, tumors require increased supply of oxygen and nutrients which is accomplished by angiogenesis, the formation of new blood vessels from pre-existing vasculature, for example, from capillaries or venules (13, 14). This transition from the avascular to the angiogenic phase of tumor growth is often referred to as the “angiogenic switch” (13, 14). The angiogenic switch and the subsequent increase in tumor blood vessel density is the most critical mechanism which allows tumors to overcome growth limitations due to insufficient blood supply. Despite extensive studies focused on tumor growth and tumor induced angiogenesis (Reviewed in (15-17), the cellular and molecular mechanisms involved are far from understanding.

Availability of Cav-1 knockout (Cav-1 KO) mice generated by several independent research laboratories allowed for extensive characterization of the role of Cav-1 in tumor growth and tumor-induced angiogenesis (18-23) (Reviewed in (24)). However, to the best of our knowledge the role of Cav-2 expressed within the tumor microenvironment in tumor growth and tumor-induced angiogenesis remained unknown. In the current study, using newly generated in our laboratory Cav-2 KO mice subjected to subcutaneous (s.c.) implantation with Lewis lung carcinoma (LLC) and B16-F10 melanoma cells, we have examined the role of host-expressed Cav-2 in regulating tumor growth and tumor growth-induced angiogenesis. Remarkably, the results of these studies determined that in contrast to wild type (WT) mice, LLC tumors are unable to grow while B16-F10 tumors display retarded growth in the host microenvironment lacking Cav-2 expression. Further studies determined impaired pathological angiogenesis in tumors implanted into Cav-2 KO mice.

Material and Methods

Cell lines

LLC and B16-F10 cell lines (ATCC) were cultured in DMEM containing 10% FBS, 1% L-glutamine and 100 UI/ml of penicillin plus streptomycin in a humidified chamber at 37C under 5% CO_2. Both cell lines were regularly authenticated according to the guidelines provided by ATCC based on morphology (rounded-loosely attached or floating for LLCs and spindle-shaped plus epithelial-like for B16-F10), viability, recovery and growth, most recently confirmed one month before use.

Mice

6-8-week old C57BL/6N Cav-2 KO and WT littermate mice originating from Charles River Laboratories were used for all experiments according to the protocol approved by the University of Missouri Animal Care and Use Committee.

Cav-2 KO mice were generated in C57BL/6N background with the assistance of Mouse Biology Program (UC Davis, CA) by deletion of entire exon 2 and a 5′ portion of exon 3 (See Supplementary Methods and Figures S1-2 for details).

Tumor cell implantation and growth

To examine the role of host-expressed Cav-2 in tumor growth, LLC or B16-F10 melanoma (10^6 cells in 100 ul phosphate-buffered saline [PBS]) were injected subcutaneously (s.c.) in the lower back right and left flanks of 6-8-week old Cav-2 KO and WT littermate mice. When tumors became palpable (typically on day 6 after implantation), LLC tumor growth was monitored every other day by measuring the length and width of the tumor using a caliper. Tumor volume was calculated using the following formula: volume = $0.52 \times (\text{width})^2 \times (\text{length})$. In addition, at the end of the experiments (typically day 17 for LLC and day 14 for B16-F10), tumors were removed and tumor mass was determined by weighing.

Immunohistochemistry

LLC tumors were resected on day 6 (the earliest palpable tumors) or day 10, while B16-F10 on day 8 of the experiment and immersed in 10% neutral formalin for overnight fixation. Fixed tissues were processed for paraffin embedment and sectioned for histochemical and immunohistochemical assays. Sections were stained with hematoxylin and eosin (H&E) for evaluation of morphological changes and with the picrosirius red method to detect the presence of extracellular collagen.

Immunohistochemical analysis was performed on paraffin sections using antibodies to Ki-67, cleaved caspase-3, CD31 and CD34. Additionally tumors were subjected to TUNEL assay according to kit directions (In situ Cell Death Detection Kit, POD; Roche Applied Science, Indianapolis, IN). Five-μm sections were mounted onto ProbeOn Plus microscope slides (Fisher Scientific Inc., Pittsburgh, PA). Prior to immunohistochemical analysis, sections were de-waxed in xylene, rehydrated through graded concentrations of ethanol, and rinsed in distilled water. Antigen retrieval was performed by heating sections in 10 mM citrate buffer (pH 6.0) for 20 min. Slides were treated with 3% hydrogen peroxide (to inactivate endogenous peroxidase activity), and rinsed prior to incubation in blocking buffer of 5% bovine serum albumin for 20 min. Sections were then incubated for 60 min at room temperature with each of the following primary antibodies: anti-CD31 antibody (1:50-1:100 dilution of a rabbit anti-CD31 polyclonal antibody [ab28364] Abcam, Inc., Cambridge, MA); anti-CD34 antibody (1:100 dilution of a rat anti-CD34 monoclonal antibody [MEC-14.7, ab8158], Abcam); anti-Ki-67 antibody (1:300 dilution of a rabbit anti-Ki-67 polyclonal [RB1510-P]; Thermo Scientific, Fremont, CA); and anti-cleaved caspase-3, (1:100 dilution of a rabbit anti-cleaved caspase-3 polyclonal antibody [ASP 175, #9661], Cell Signaling Technology, Beverly, MA). To detect the antibodies to CD34, sections were incubated for 30 minutes with a biotinylated secondary antibody (rabbit anti-rat IgG,

DAKO, Carpenteria, CA) and then for 30 minutes with a streptavidin-linked horseradish peroxidase product (DAKO). Sections probed with antibodies to CD31, Ki-67 and cleaved caspase-3, were incubated with EnVision®, a horseradish peroxidase-labeled polymer conjugated to anti-rabbit antibodies (DAKO). Bound antibodies were visualized following incubation with 3,3′-diaminobenzidine solution (0.05% with 0.015% H2O2 in PBS; DAKO) for 3-5 minutes. Sections were counterstained with Mayer's hematoxylin, dehydrated, and cover-slipped for microscopic examination. Images were captured using Anxiovert IX70 microscope with 20× objective.

Immunoblotting

Lung and LLC tumor tissue was extracted from mice and snap-frozen with liquid nitrogen followed by extraction with tissue grinder and lysed in a RIPA lysis buffer containing: 50 mM Tris HCl, 0.1 mM EGTA, 0.1 mM EDTA, 100 mM leupeptin, 1 mM phenylmethylsulfonyl fluoride, 1% (vol/vol) NP-40, 0.1% SDS, and 0.5% deoxycholic acid; pH 7.4, homogenized, and centrifuged for 10 min at 14,000 rpm and at 4C. Insoluble material was removed and the supernatants were then mixed with Laemmli SDS loading buffer and boiled. Samples were subjected to SDS-PAGE and immmunoblotting as described previously (7, 8). Briefly, an equal protein amount was loaded on SDS-PAGE, and proteins were electro-transferred onto nitrocellulose membranes. The membranes were washed in Tris-buffered saline with 0.1% Tween, blocked in 5% milk, and incubated with primary antibodies against Cav-2, Hsp-90 (from BD Transduction Laboratories), total endothelial nitric oxide synthase eNOS (from Abcam), phospho-serine 1177-eNOS (P-S1177-eNOS), cleaved caspase-3 (from Cell Signaling), thrombospondin-1 (TSP-1) or Poly ADP ribose polymerase-1 (PARP-1) (from Santa Cruz) at 4°C overnight followed by incubation with horseradish peroxidase labeled secondary goat anti-mouse antibody (Biorad), and developed by enhanced chemiluminescence. Where appropriate, the densitometric values for specific immunoblots were determined using Image J followed by calculating and expressing densitometric ratios as mean ± S.D. from two replications based on one representative out of two total experiments.

RNA isolation and analysis of specific gene expression by quantitative real time PCR

Quantitative real time PCR (qRT-PCR) – qRT-PCR was performed similar to described previously (7, 8) with minor modifications (see Supplementary Methods for detailed description).

Statistical analyses

For the experiments involving time dependent growth of LLC tumor grafts the data are expressed as mean ± S.E.M. (n=6-8). To determine the statistical significance, the two-way analysis of variance (ANOVA) was used followed by Bonferroni post-hoc test. For all other experiments Student's t-test was performed. Differences were considered statistically significant (*) at $p<0.05$.

Results

Host deficiency in Cav-2 results in defective and retarded subcutaneous tumor growth using syngeneic mouse LLC and B16-F10 melanoma models, respectively

To examine the role of host expressed Cav-2 in tumor growth, LLC cells were implanted into WT and Cav-2 KO male mice and tumor growth was determined as described in experimental procedures. As expected, the volume of LLC tumors progressively increased in WT mice reaching ca. 17.1 ± 6.4, 51.4 ± 24.3, 69.6 ± 18.4, 94.8 ± 18.7, 201 ± 38, and 371.5 ± 136.9 mm^3 (n=8) on day 6, 8, 10, 12, 14, and 17, respectively (Fig. 1A; closed squares). Remarkably, in contrast to WT mice, LLC tumors implanted into Cav-2 KO mice did not display a significant growth gradually regressed, in particular between day 10 and 17 (Fig. 1A; open squares). Specifically, the volume of LLC tumors in Cav-2 KO mice reached ca. 15.5 ± 5.4, 30 ± 8.2, 23 ± 12.8, 13.2 ± 11.0, 8.8 ± 6.6, and 2.1 ± 2.1 mm^3 on day 6, 8, 10, 12, 14, and 17, respectively (Fig. 1A; open squares). The dramatic reduction in the volume of Cav-2 KO LLC tumors on day 17 was independently confirmed upon surgical removal followed by photographing (Fig. 1B) and weighing. Specifically, the average tumor mass was ca. 285 ± 86 mg (n=6) and only 0.9 ± 0.3 mg (n=6) for WT and Cav-2 KO mice, respectively (Fig. 1C), indicating significant ($P<0.0001$), nearly a 320-fold reduction of LLC tumor mass in Cav-2 KO compared to WT mice at day 17. To determine if the defective LLC tumor growth in Cav-2 KO mice was permanent, four additional Cav-2 KO mice were maintained up to 2 months after LLC tumor implantation into two flanks per mouse (n=8). All eight LLC tumors implanted into Cav-2 mice completely regressed and mice remained tumor free within this prolonged time frame (not shown), suggesting that host-expressed Cav-2 is required for LLC tumor growth. To test if the observed defect in LLC tumor growth was gender dependent or independent, in addition to male mice (shown in Fig. 1) we have also tested female mice. Similar to Cav-2 KO male mice, Cav-2 KO female mice also displayed defective LLC tumor growth (Fig. S3). To determine if the role of host expressed Cav-2 is restricted to LLC model or is more global, we used B16-F10 melanoma cells as an additional syngeneic model of subcutaneous tumor growth in C57BL6 mice. Our results showed statistically significant ($P<0.05$) nearly 3-fold reduction in B16-F10 tumor growth in Cav-2 KO compared to WT mice at final day 14 of the experiment (Fig. S4). Taken together, our data suggests that host Cav-2 deficiency negatively affects subcutaneous tumor growth in both LLC and B16-F10 models in vivo.

Host deficiency in Cav-2 results in reduced microvascular density (MVD) within LLC and B16-F10 tumors

Since angiogenesis is critical for tumor growth, we hypothesized that the defective tumor growth in Cav-2 KO mice should be associated with reduced MVD within tumor tissue. To test our hypothesis, LLC tumors were extracted on day 10 of the experiment, i.e., before the largest tumors from WT mice reached maximal volume of ca. 100 mm^3 and no statistically significant difference in tumor volume could be observed between WT and Cav-2 KO (See Fig. 1A). To determine MVD within LLC tumor tissue, 5-um paraffin sections were immunohistochemically stained with anti-CD31 and anti-CD34 antibodies. As shown in Fig. 2AB, Cav-2 KO tumors had considerably less CD31 positive structures (Fig. 2B) compared to WT counterparts (Fig. 2A). Similar to CD31, Cav-2 KO tumors also displayed reduced

numbers of CD34 positive structures (Fig. 2F) compared to WT counterparts (Fig. 2E). Quantitative analysis revealed that Cav-2 KO tumors had significantly, ca.13.2-fold reduced number of CD31 positive vessels (Fig. 2C) and ca. 8.5-fold reduced CD31 positive vessel area (Fig. 2D). Cav-2 KO tumors had also significantly, ca.3.5-fold reduced number of CD34 positive vessels (Fig. 2G) and ca. 3.6-fold reduced CD34 positive vessel area (Fig. 2H).

To determine MVD in B16-F10 melanoma tumors, staining with anti-CD31 antibody was performed on paraffin sections from smaller tumors extracted at day 8 of the experiment (Fig. S5A-B). Quantitative analysis revealed significant, ca. 2.5-fold reduction in the number of CD31 positive vessels in B16-F10 tumors implanted into Cav-2 KO compared to WT mice (Fig. S5C). Taken together, our data indicate impaired angiogenesis within LLC and B16-F10 tumors implanted into Cav-2 KO compared to WT mice.

Host deficiency in Cav-2 results in reduced cell proliferation within LLC tumors

To determine if the defective LLC tumor growth in Cav-2 KO mice is associated with reduced cell proliferation within tumor tissue 5-um paraffin sections from tumors extracted on day 10 were immunohistochemically stained with anti-Ki-67 antibody. As shown in Fig. 3, there was visibly reduced density of Ki-67 positive cells in LLC tumors implanted in Cav-2 KO (Fig. 3B) compared to WT mice (Fig. 3A). Quantitative analysis revealed significant ($P<0.0001$), ca.3.6-fold reduction of Ki-67 positive nuclei in LLC tumors implanted into Cav-2 KO (71.3 ± 7.41; $n=6$) compared to WT mice (254 ± 22.0; $n=7$) (Fig. 3C). Our data with Ki-67 staining suggests reduced cell proliferation within LLC tumors 10 days after implantation into Cav-2 KO mice.

Host deficiency in Cav-2 results in increased fibrosis within LLC tumors

To determine the degree of fibrosis within tumors extracted on day 10 of the experiment, 5-um paraffin sections were histochemically stained with PSR known to quantitatively detect extracellular collagen. In contrast to WT tumors in which very little PSR positive signal could be observed (Fig. 3D), Cav-2 KO tumors displayed considerable staining with PSR (Fig. 3E). As shown in Fig. 3F, quantitative analysis revealed significant ($P<0.0001$), ca. 13.3-fold increase of PSR positive area in LLC tumors implanted into Cav-2 KO (20.8 ± 2.86; $n=8$) compared to WT mice (1.56 ± 0.471; $n=8$). Taken together, our data with PSR staining suggests increased deposition of extracellular collagen and fibrosis within LLC tumors implanted into Cav-2 KO mice.

Host deficiency in Cav-2 results in increased necrotic death within LLC tumors

To examine if defective LLC tumor growth (Fig. 1) could also be associated with increased cellular apoptosis, 5-um sections from LLC tumors extracted on day 10 were stained with anti-cleaved caspase-3 antibody (marker of early apoptosis) as well as subjected to TUNEL staining which detects late apoptosis (intense staining of DNA fragmentation localized within cell nuclei) as well non-apoptotic cellular death (25) (intense whole cell staining). Interestingly, although a limited number of cells was intensely stained with cleaved caspase-3 antibody in WT tumors (Fig. 4A), no clearly cleaved caspase-3 positive cells could be observed within Cav-2 KO tumors (Fig. 4B). Consistent with cleaved caspase-3, a

limited number of cells with intense nuclear TUNEL staining could be observed in WT tumors (Fig. 4C). However, in contrast to cleaved caspase-3, nearly all cells within Cav-2 KO tumors displayed intense, whole cell staining with TUNEL (Fig. 4D), suggesting massive non-apoptotic cell death within LLC tumors 10 days after implantation into Cav-2 KO mice. H&E staining of 5-um paraffin sections from tumors extracted on day 10 revealed that in contrast to WT, in which hematoxylin-stained nuclei were intact and clearly distinguishable (Fig. 4E), the cellular/nuclear integrity in Cav-2 KO samples were compromised (Fig. 4F), suggesting massive cellular cell death within Cav-2 KO tumors. To shed more light on the mechanism of cell death in Cav-2 KO LLC tumors, we used immunoblotting with anti-cleaved caspase-3 antibody of tumor lysates generated between day 6 and 10 after implantation. Consistent with immunohistochemistry data, the levels of cleaved caspase-3 were reduced in Cav-2 KO compared to WT LLC tumors in a time-dependent manner (Fig. 4G), suggesting diminished apoptotic signaling and caspase-3-independent death in Cav-2 KO LLC tumors. We then examined the expression levels of 50 kDa necrotic cleavage fragment of PARP-1 (26) and determined time-dependent increase in Cav-2 KO compared to WT LLC tumors (Fig. 4G; central immunoblot and 4H. Overall, our immunohistochemistry and immunoblotting data suggest massive necrotic cell death within LLC tumors implanted into Cav-2 KO mice.

Host deficiency in Cav-2 reduces MVD but does not affect cell proliferation and cell death within the earliest palpable LLC tumors

To determine if reduced MVD in LLC tumors implanted into Cav-2 KO is causative rather than a consequence of reduced proliferation and increased death observed on day 10 after tumor implantation (Figs: 2, 3A-C and 4), we shifted our focus to the earliest palpable LLC tumors (6 days after implantation). Specifically, 5-um paraffin sections of the earliest palpable LLC tumors were immunohistochemically stained with antibodies against CD31 and Ki-67 as well as with TUNEL (Fig. 5A-H) or histochemically stained with H&E to assess the general cell morphology. As shown in Fig. 5A-C, the earliest palpable Cav-2 KO tumors already displayed visibly reduced MVD determined based on anti-CD31 staining (Fig. 5B) compared to WT counterparts (Fig. 5A). Quantitative analysis determined that the earliest palpable Cav-2 KO tumors had significantly ($P<0.0001$), ca.2.6-fold reduced number of CD31 positive vessels per field (Fig. 5C). Remarkably, in contrast to reduced MVD, no significant difference in proliferation determined based on Ki-67 positive staining (Fig. 5D-F) nor significant difference in cell death assessed by TUNEL staining (Fig. 5G-I) could be observed between the earliest palpable WT and Cav-2 KO tumors (6 days after implantation). Consistent with similar cell proliferation and survival rate, H&E staining revealed relatively similar cell morphology in the earliest palpable LLC tumors implanted in WT (Fig. 5J) and in Cav-2 KO mice (Fig. 5K). Taken together, our data with reduced MVD but unaltered cell proliferation and death in the earliest palpable Cav-2 KO tumors suggest that host deficiency in Cav-2 results in reduced LLC tumor-induced angiogenesis prior to decreased LLC tumor cell proliferation/survival. Thus impaired LLC tumor-induced angiogenesis is the causative mechanism responsible for reduced cell proliferation/survival and consequent defective LLC tumor growth in Cav-2 KO mice.

Host deficiency in Cav-2 increases expression levels of thrombospondin-1 and inhibits serine 1177 phosphorylation of endothelial nitric oxide synthase within LLC tumors

To determine molecular mechanisms responsible for reduced angiogenesis associated with defective LLC tumor growth, we performed qRT-PCR of mRNA levels for selected known factors involved in angiogenesis in tumors extracted 6 days after implantation. No appreciable differences in mRNA levels were observed for pro-angiogenic growth factors such as VEGF-A (Fig. S6A) or PlGF (Fig. S6B), while a non-significant trend for reduced mRNA levels of FGF-2, TGF-transcriptional targets of Notch pathway Hes-1 and Hey-1 in Cav-2 KO LLC tumors was observed (Fig. S6C-F).

In contrast to the previously mentioned growth factors and transcriptional targets of Notch, there was significant, ca. 1.9-fold increase in mRNA level of anti-angiogenic thrombospondin-1 (TSP-1) on day 6 (Fig. 6A). Analysis of tumors extracted at later time points, i.e., days 8 and 10 determined highly significant ca. 2.4- and 4-fold increase in TSP-1 mRNA in Cav-2 KO tumors (Fig. 6B-C). The time-dependent increase in TSP-1 in Cav-2 KO compared to WT tumors was also observed at protein level using immunoblotting approach (Fig. 6D; top immunoblot and 6E). Next, we examined serine 1177 phosphorylation of endothelial nitric oxide synthase (P-S1177-eNOS) because it is important endothelial-specific target for TSP-1 which is involved in tumor angiogenesis and permeability (Reviewed by (27). Remarkably, we observed profound time-dependent reduction in the levels of phospho-S1177-eNOS within Cav-2 KO tumors (Fig. 6D; 2nd immunoblot from the top and 6F). Since VEGFR2 pathway activation in tumor endothelial cells is critical for tumor-induced angiogenesis, we performed immunoblotting with anti-phospho-Y1175-VEGFR2 antibody (Cell Signaling) but were unable to detect a reliable signal within tumor lysates (not shown). However, consistent with reduced angiogenesis, we detected time-dependent reduction in expression levels of total VEGFR2 in Cav-2 KO tumors (Fig. 6D; 4th immunoblot from the top). Taken together, our data suggests that host deficiency in Cav-2 results in increased expression of anti-angiogenic TSP-1 and inhibition of phospho-S1177-eNOS.

Discussion

In this study using newly generated mice with global loss of Cav-2 we show for the first time that LLC cells subcutaneously implanted into Cav-2 KO mice display defective tumor growth and angiogenesis. In addition, our studies reveal reduced tumor growth and angiogenesis using an independent syngeneic model involving B16-F10 melanoma cells. Moreover, we demonstrate that impaired tumor-induced angiogenesis is responsible for defective LLC tumor growth. Finally, we identify increased levels of anti-angiogenic TSP-1 as well as impaired S1177 phosphorylation of eNOS as likely molecular mechanisms associated with defective LLC tumor growth and angiogenesis in Cav-2 KO mice.

The failure of LLC tumors to grow in Cav-2 KO mice is remarkable. In particular, the fact that LLC tumors implanted in Cav-2 KO mice not only grew much slower than their WT counterparts within the earlier phase, i.e., up to ca. ten days after implantation, but that they showed a clear regression pattern within a typical experimental time frame of up to seventeen days, and that all Cav-2 KO mice were tumor free when left for a period of up to

two months after implantation, suggests that host-expressed Cav-2 is absolutely necessary for LLC tumor growth within subcutaneous environment. Interestingly, while growth of B16 was significantly slower in Cav-2 KO mice, the phenotype was less robust, suggesting a greater ability of host-expressed Cav-2 to promote growth of LLC than B16 melanoma skin grafts.

The data showing tumor-promoting role of host-expressed Cav-2 is in agreement with several clinical observations involving various human cancers. For instance, Cav-2 expression was up-regulated in esophageal (28) and urothelial carcinoma of the urinary bladder (29, 30). Moreover, Cav-2 expression was closely associated with basal-like immunophenotype and proved to be a prognostic factor of breast cancer (31, 32). The expression levels of Cav-2 were also upregulated during prostate cancer progression (33). Another study reported a strong correlation between Cav-2 negativity within tumors and a 5-year survival of patients with stage I lung adenocarcinoma and multivariate analyses taking into account the age and asbestos fiber content revealed that Cav-2 positivity might be an independent unfavorable prognostic factor (34). In addition to the previously discussed published clinical studies, several datasets available through searchable database cBioPortal (35, 36) indicate Cav-2 gene amplification in other tumor types such as glioblastoma, ovarian serous cystadenocarcinoma, stomach adenocarcinoma, or melanoma. Thus in light of the previously discussed clinical data and our new data with defective or retarded subcutaneous tumor growth in Cav-2 KO mice using LLC and B16-F10 syngeneic tumor models, future mechanistic studies examining the role of Cav-2 expressed in tumor cells versus tumor microenvironment in regulating tumor progression are clearly warranted.

The data showing markedly reduced MVD within tumors implanted in Cav-2 KO mice and when WT tumors were still very small, strongly suggests that Cav-2 expressed in tumor microenvironment promotes pathological angiogenesis induced in LLC and B16-F10 models. In addition, an obviously reduced cell proliferation and enhanced cell death as well fibrosis within LLC tumors observed ten days after implantation in Cav-2 KO mice is consistent with inability of LLC skin grafts to grow in Cav-2-deficient microenvironment. However, given that LLC tumors extracted from Cav-2 KO mice ten days after implantation, in addition to robustly diminished MVD appear to display a massive cell death and fibrosis, the question remained as to whether a defective angiogenesis is the primary mechanism and a cause, simply coincides, or is a consequence of reduced proliferation and enhanced cell death as well as fibrosis within LLC tumors. To answer the latter question, we performed additional experiments involving the earliest palpable tumors extracted from WT and Cav-2 KO mice only six days after LLC implantation. These experiments determined significantly reduced MVD but comparable cell proliferation and survival within the earliest palpable LLC tumors implanted into Cav-2 KO mice, indicating that defective angiogenesis occurs prior to reduced cell proliferation and survival. Thus ability to promote pathological angiogenesis and the consequent enhancement of tumor cell proliferation and survival is the critical mechanism via which Cav-2 expressed within tumor microenvironment drives tumor growth. Overall, our data with defective angiogenesis being responsible for the inability of LLC tumors to grow within Cav-2 KO microenvironment is consistent with the notion that angiogenesis plays an important role in the tumor growth and its blood supply (13, 14, 16, 17).

What are the molecular mechanisms responsible for impaired tumor induced angiogenesis and inhibition of tumor growth in Cav-2 KO mice? Since TSP-1 is the major anti-angiogenic factor most extensively characterized in the tumor microenvironment (Reviewed in (37)), it is plausible that time-dependent upregulation of TSP-1 at mRNA and protein levels observed within LLC tumors implanted into Cav-2 KO mice is an important molecular mechanism via which host deficiency in Cav-2 inhibits tumor angiogenesis and growth. While TSP-1 was reported to inhibit angiogenesis via multiple mechanisms, inhibition of endothelial cell-specific VEGR2- and eNOS-dependent pathway(s) appear to be prominent (27, 37). Endothelial cell-expressed VEGFR2-dependent pathway is particularly important in tumor angiogenesis (16, 17, 38). Notably, TSP-1 was shown to regulate VEGFR2 phosphorylation at Y1175 and overall VEGFR2 signaling in endothelial cells (39, 40). Thus, using immunohistochemistry and immunoblotting approaches we attempted to compare phospoho-Y1175-VEGFR2 levels but were unable to detect specific signal in tumor samples (not shown). Hence to further examine activation of VEGR2-dependent pathway within LLC tumors, we next focused on phospho-S1177-eNOS which is an important endothelial-specific downstream target of phospoho-Y1175-VEGFR2 and is key for VEGFR2-dependent angiogenesis and permeability (41-44). Remarkably, we observed robust suppression of phospho-S1177-eNOS, which closely correlated with upregulation of TSP-1 within LLC tumors implanted into Cav-2 KO mice, suggesting impaired S1177-eNOS phosphorylation as a likely consequence of inhibition of VEGFR2-dependent pathway by TSP-1. Future mechanistic studies examining how host Cav-2 deficiency upregulates TSP-1within tumor microenvironment are clearly warranted.

While global Cav-2 KO mice are ideal model to determine the role of host-expressed Cav-2 in tumor growth and tumor growth-induced pathological angiogenesis, future studies involving various cell type/tissue-specific rescue of Cav-2 in global Cav-2 KO background will be helpful to unequivocally determine cell-type(s)-specific and more detailed molecular mechanisms involved in tumor angiogenesis and tumor growth-promoting role of Cav-2. In addition, it will also be interesting to determine the significance of Cav-2 in additional mouse models of cancer, in particular in orthotopic models of tumor growth and metastasis.

Anti-angiogenic therapy is a very important strategy in cancer treatment, however, due to frequently developed resistance, for instance to anti-VEGF therapy, identifying additional targets for anti-angiogenic therapy is crucial (15). Therefore, our new data showing that Cav-2 expressed in host microenvironment promotes tumor induced angiogenesis suggest that Cav-2 could possibly be an important target for anti-angiogenic therapy and cancer treatment and thus require further investigation. Moreover, except hyperproliferation involving Flk-1 (VEGFR2)-positive cells in the lung, Cav-2 KO mice generated by Lisanti's group (45) and our group are healthy, reproduce normally, and do not display major defects in physiological angiogenesis. Thus targeting Cav-2 could possibly selectively disrupt tumor microvessels without affecting normal vasculature.

Supplementary Material

Refer to Web version on PubMed Central for supplementary material.

Acknowledgments

Financial support: This work was supported by the grant from the National Institute of Health (1R01HL081860 to GS).

References

1. Williams TM, Lisanti MP. The Caveolin genes: from cell biology to medicine. Ann Med. 2004; 36:584–95. [PubMed: 15768830]
2. Scherer PE, Okamoto T, Chun M, Nishimoto I, Lodish HF, Lisanti MP. Identification, sequence, and expression of caveolin-2 defines a caveolin gene family. Proc Natl Acad Sci U S A. 1996; 93:131–5. [PubMed: 8552590]
3. Sowa G. Novel insights into the role of caveolin-2 in cell- and tissue-specific signaling and function. Biochemistry research international. 2011; 2011:809259. [PubMed: 22229094]
4. Yamasaki T, Seki N, Yoshino H, Itesako T, Hidaka H, Yamada Y, et al. MicroRNA-218 inhibits cell migration and invasion in renal cell carcinoma through targeting caveolin-2 involved in focal adhesion pathway. J Urol. 2013; 190:1059–68. [PubMed: 23454155]
5. de Almeida CJ, Jasmin JF, Del Galdo F, Lisanti MP. Genetic ablation of caveolin-2 sensitizes mice to bleomycin-induced injury. Cell Cycle. 2013; 12:2248–54. [PubMed: 24067367]
6. Sowa G. Caveolae, caveolins, cavins, and endothelial cell function: new insights. Frontiers in physiology. 2012; 2:120. [PubMed: 22232608]
7. Abel B, Willoughby C, Jang S, Cooper L, Xie L, Vo-Ransdell C, et al. N-terminal tyrosine phosphorylation of caveolin-2 negates anti-proliferative effect of transforming growth factor beta in endothelial cells. FEBS Lett. 2012; 586:3317–23. [PubMed: 22819829]
8. Xie L, Vo-Ransdell C, Abel B, Willoughby C, Jang S, Sowa G. Caveolin-2 is a negative regulator of anti-proliferative function and signaling of transforming growth factor-beta in endothelial cells. Am J Physiol Cell Physiol. 2011; 301:C1161–74. [PubMed: 21832243]
9. Shatseva T, Lee DY, Deng Z, Yang BB. MicroRNA miR-199a-3p regulates cell proliferation and survival by targeting caveolin-2. J Cell Sci. 2011; 124:2826–36. [PubMed: 21807947]
10. Lee S, Kwon H, Jeong K, Pak Y. Regulation of cancer cell proliferation by caveolin-2 down-regulation and re-expression. Int J Oncol. 2011; 38:1395–402. [PubMed: 21373752]
11. de Almeida CJ, Witkiewicz AK, Jasmin JF, Tanowitz HB, Sotgia F, Frank PG, et al. Caveolin-2-deficient mice show increased sensitivity to endotoxemia. Cell Cycle. 2011; 10:2151–61. [PubMed: 21670588]
12. Xie L, Frank PG, Lisanti MP, Sowa G. Endothelial cells isolated from caveolin-2 knockout mice display higher proliferation rate and cell cycle progression relative to their wild-type counterparts. Am J Physiol Cell Physiol. 2010; 298:C693–701. [PubMed: 20007452]
13. Folkman J. What is the evidence that tumors are angiogenesis dependent? J Natl Cancer Inst. 1990; 82:4–6. [PubMed: 1688381]
14. Hanahan D, Folkman J. Patterns and emerging mechanisms of the angiogenic switch during tumorigenesis. Cell. 1996; 86:353–64. [PubMed: 8756718]
15. Vasudev NS, Reynolds AR. Anti-angiogenic therapy for cancer: current progress, unresolved questions and future directions. Angiogenesis. 2014; 31:31.
16. Gomes FG, Nedel F, Alves AM, Nor JE, Tarquinio SB. Tumor angiogenesis and lymphangiogenesis: tumor/endothelial crosstalk and cellular/microenvironmental signaling mechanisms. Life Sci. 2013; 92:101–7. [PubMed: 23178150]
17. Potente M, Gerhardt H, Carmeliet P. Basic and therapeutic aspects of angiogenesis. Cell. 2011; 146:873–87. [PubMed: 21925313]
18. Chang SH, Feng D, Nagy JA, Sciuto TE, Dvorak AM, Dvorak HF. Vascular permeability and pathological angiogenesis in caveolin-1-null mice. Am J Pathol. 2009; 175:1768–76. [PubMed: 19729487]
19. Dewever J, Frerart F, Bouzin C, Baudelet C, Ansiaux R, Sonveaux P, et al. Caveolin-1 is critical for the maturation of tumor blood vessels through the regulation of both endothelial tube formation and mural cell recruitment. Am J Pathol. 2007; 171:1619–28. [PubMed: 17916598]

20. Lin MI, Yu J, Murata T, Sessa WC. Caveolin-1-deficient mice have increased tumor microvascular permeability, angiogenesis, and growth. Cancer Res. 2007; 67:2849–56. [PubMed: 17363608]
21. Tahir SA, Yang G, Goltsov AA, Watanabe M, Tabata K, Addai J, et al. Tumor cell-secreted caveolin-1 has proangiogenic activities in prostate cancer. Cancer Res. 2008; 68:731–9. [PubMed: 18245473]
22. Woodman SE, Ashton AW, Schubert W, Lee H, Williams TM, Medina FA, et al. Caveolin-1 knockout mice show an impaired angiogenic response to exogenous stimuli. Am J Pathol. 2003; 162:2059–68. [PubMed: 12759260]
23. Yang G, Addai J, Wheeler TM, Frolov A, Miles BJ, Kadmon D, et al. Correlative evidence that prostate cancer cell-derived caveolin-1 mediates angiogenesis. Hum Pathol. 2007; 38:1688–95. [PubMed: 17707459]
24. Sowa, G. Caveolins in Tumor Angiogenesis. Caveolins in Cancer Pathogenesis, Prevention and Therapy. Mercier, I.; Jasmin, J-F.; Lisanti, MPP., editors. Springer; New York: 2012. p. 75-90.
25. Collins RJ, Harmon BV, Gobe GC, Kerr JF. Internucleosomal DNA cleavage should not be the sole criterion for identifying apoptosis. Int J Radiat Biol. 1992; 61:451–3. [PubMed: 1349327]
26. Gobeil S, Boucher CC, Nadeau D, Poirier GG. Characterization of the necrotic cleavage of poly(ADP-ribose) polymerase (PARP-1): implication of lysosomal proteases. Cell Death Differ. 2001; 8:588–94. [PubMed: 11536009]
27. Isenberg JS, Martin-Manso G, Maxhimer JB, Roberts DD. Regulation of nitric oxide signalling by thrombospondin 1: implications for anti-angiogenic therapies. Nat Rev Cancer. 2009; 9:182–94. [PubMed: 19194382]
28. Hu YC, Lam KY, Law S, Wong J, Srivastava G. Profiling of differentially expressed cancer-related genes in esophageal squamous cell carcinoma (ESCC) using human cancer cDNA arrays: overexpression of oncogene MET correlates with tumor differentiation in ESCC. Clin Cancer Res. 2001; 7:3519–25. [PubMed: 11705871]
29. Fong A, Garcia E, Gwynn L, Lisanti MP, Fazzari MJ, Li M. Expression of caveolin-1 and caveolin-2 in urothelial carcinoma of the urinary bladder correlates with tumor grade and squamous differentiation. Am J Clin Pathol. 2003; 120:93–100. [PubMed: 12866378]
30. Dubosq F, Ploussard G, Soliman H, Turpin E, Latil A, Desgrandchamps F, et al. Identification of a three-gene expression signature of early recurrence in non-muscle-invasive urothelial cell carcinoma of the bladder. Urol Oncol. 2012; 30:833–40. [PubMed: 21489836]
31. Elsheikh SE, Green AR, Rakha EA, Samaka RM, Ammar AA, Powe D, et al. Caveolin 1 and Caveolin 2 are associated with breast cancer basal-like and triple-negative immunophenotype. Br J Cancer. 2008; 99:327–34. [PubMed: 18612310]
32. Savage K, Leung S, Todd SK, Brown LA, Jones RL, Robertson D, et al. Distribution and significance of caveolin 2 expression in normal breast and invasive breast cancer: an immunofluorescence and immunohistochemical analysis. Breast Cancer Res Treat. 2008; 110:245–56. [PubMed: 17912630]
33. Gould ML, Williams G, Nicholson HD. Changes in caveolae, caveolin, and polymerase 1 and transcript release factor (PTRF) expression in prostate cancer progression. Prostate. 2010; 70:1609–21. [PubMed: 20564315]
34. Wikman H, Seppanen JK, Sarhadi VK, Kettunen E, Salmenkivi K, Kuosma E, et al. Caveolins as tumour markers in lung cancer detected by combined use of cDNA and tissue microarrays. J Pathol. 2004; 203:584–93. [PubMed: 15095482]
35. Cerami E, Gao J, Dogrusoz U, Gross BE, Sumer SO, Aksoy BA, et al. The cBio cancer genomics portal: an open platform for exploring multidimensional cancer genomics data. Cancer Discov. 2012; 2:401–4. [PubMed: 22588877]
36. Gao J, Aksoy BA, Dogrusoz U, Dresdner G, Gross B, Sumer SO, et al. Integrative analysis of complex cancer genomics and clinical profiles using the cBioPortal. Sci Signal. 2013; 6:2004088.
37. Lawler PR, Lawler J. Molecular basis for the regulation of angiogenesis by thrombospondin-1 and -2. Cold Spring Harb Perspect Med. 2012; 2
38. Olsson AK, Dimberg A, Kreuger J, Claesson-Welsh L. VEGF receptor signalling - in control of vascular function. Nat Rev Mol Cell Biol. 2006; 7:359–71. [PubMed: 16633338]

39. Zhang X, Kazerounian S, Duquette M, Perruzzi C, Nagy JA, Dvorak HF, et al. Thrombospondin-1 modulates vascular endothelial growth factor activity at the receptor level. FASEB J. 2009; 23:3368–76. [PubMed: 19528255]
40. Kaur S, Martin-Manso G, Pendrak ML, Garfield SH, Isenberg JS, Roberts DD. Thrombospondin-1 inhibits VEGF receptor-2 signaling by disrupting its association with CD47. J Biol Chem. 2010; 285:38923–32. [PubMed: 20923780]
41. Dimmeler S, Fleming I, Fisslthaler B, Hermann C, Busse R, Zeiher AM. Activation of nitric oxide synthase in endothelial cells by Akt-dependent phosphorylation. Nature. 1999; 399:601–5. [PubMed: 10376603]
42. Fulton D, Gratton JP, McCabe TJ, Fontana J, Fujio Y, Walsh K, et al. Regulation of endothelium-derived nitric oxide production by the protein kinase Akt. Nature. 1999; 399:597–601. [PubMed: 10376602]
43. Dimmeler S, Dernbach E, Zeiher AM. Phosphorylation of the endothelial nitric oxide synthase at ser-1177 is required for VEGF-induced endothelial cell migration. FEBS Lett. 2000; 477:258–62. [PubMed: 10908731]
44. Fukumura D, Gohongi T, Kadambi A, Izumi Y, Ang J, Yun CO, et al. Predominant role of endothelial nitric oxide synthase in vascular endothelial growth factor-induced angiogenesis and vascular permeability. Proc Natl Acad Sci U S A. 2001; 98:2604–9. [PubMed: 11226286]
45. Razani B, Wang XB, Engelman JA, Battista M, Lagaud G, Zhang XL, et al. Caveolin-2-deficient mice show evidence of severe pulmonary dysfunction without disruption of caveolae. Mol Cell Biol. 2002; 22:2329–44. [PubMed: 11884617]

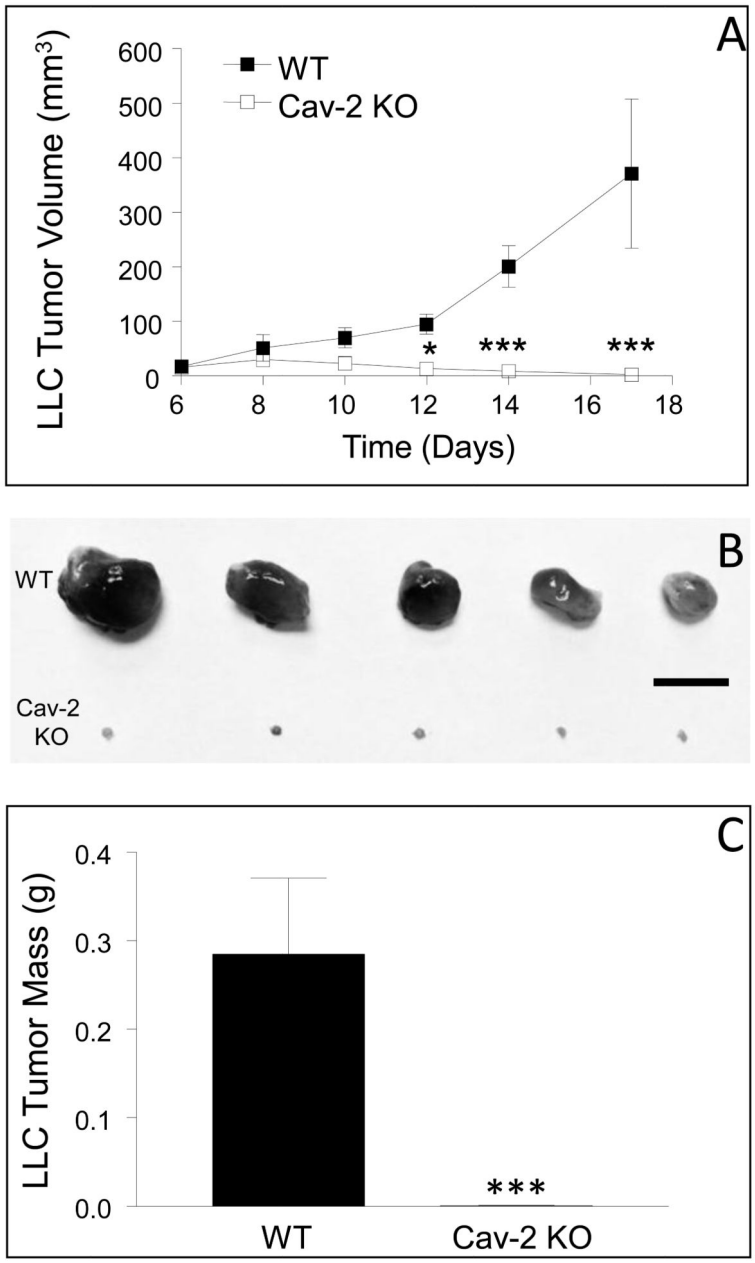

Figure 1. Subcutaneous growth of LLC tumors in WT versus Cav-2 KO male mice

To examine LLC tumor growth, LLC cells were s.c. implanted into two flanks of WT and Cav-2 KO male mice. A: Graphical representation of tumor growth monitored every 2-3 days using a caliper. LLC tumor volumes were calculated according to the formula: Volume = $0.52 \times (\text{width})^2 \times (\text{length})$. *, $P < 0.05$ and ***, $p<0.001$ compared with WT by two-way ANOVA followed by Bonferroni post-test (n=8 for WT and for Cav-2 KO). B: Representative photographs of tumors extracted from WT and Cav-2 KO mice on day 17 of the experiment. Bar: 10 mm. C: Tumors extracted on day 17 (shown in B) were weighted and the average tumor mass ± S.E.M. was calculated. ***, $P < 0.0001$ compared with WT by unpaired t-test (n = 8).

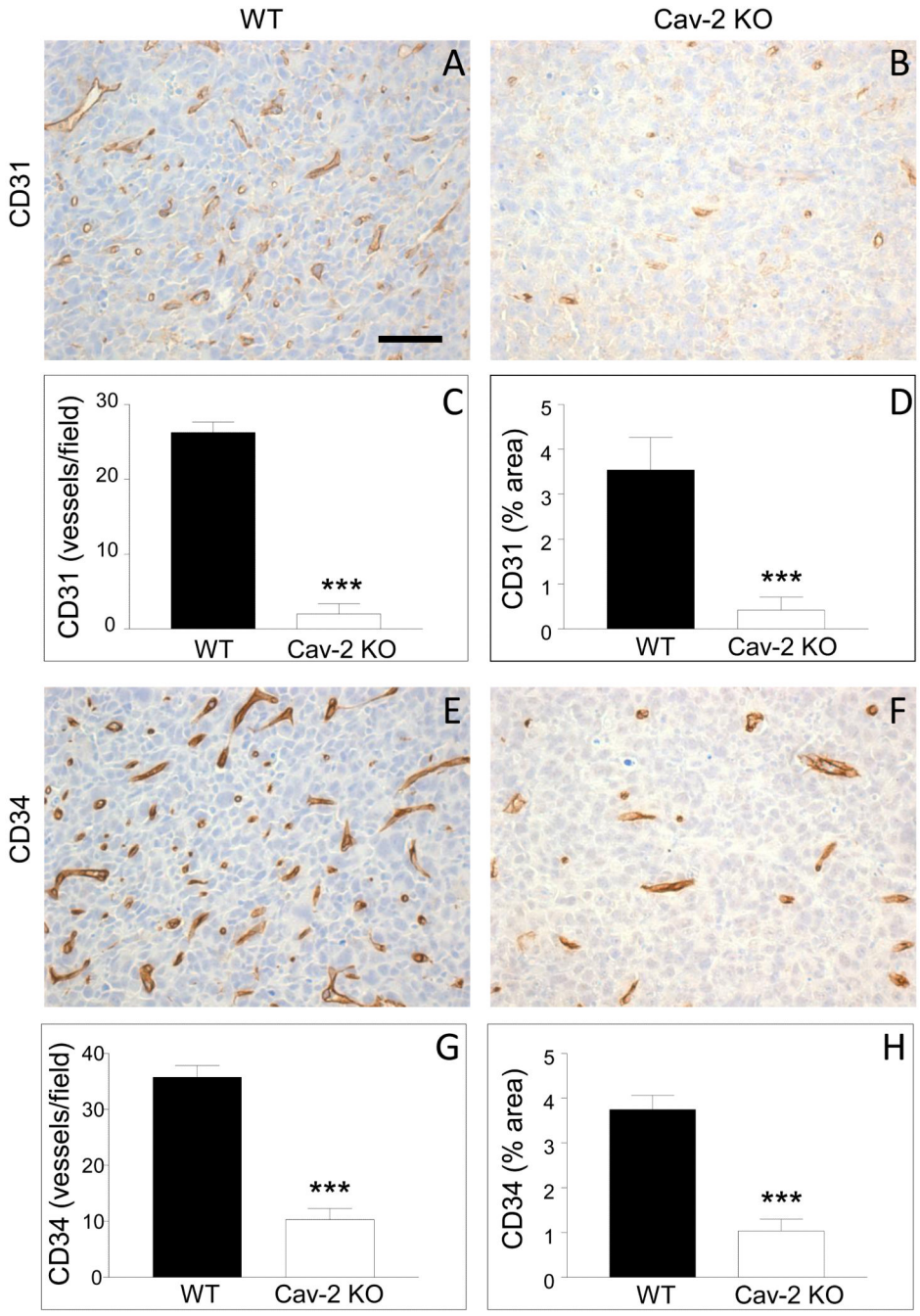

Figure 2. MVD within LLC tumors implanted into Cav-2 KO and WT mice

5-um paraffin sections of the tumor tissue extracted 10 days after s.c. implantation of LLC cells were immunohistochemically stained with antibodies against CD31 (A,B) and CD34 (E,F) as described in methods to label blood vessels. MVD within the tumors, quantified based on CD31 and CD34 positive staining is expressed as mean number of CD31 or CD34 positive vessels per field (C for CD31 and G for CD34) as well as mean % area (D for CD31 and H for CD34) ± S.E.M. ***, P<0.0001 (C, G, H) and P<0.0003 (D) compared with WT by unpaired t-test (n=12 for WT and for Cav-2 KO). Bar: 50 um.

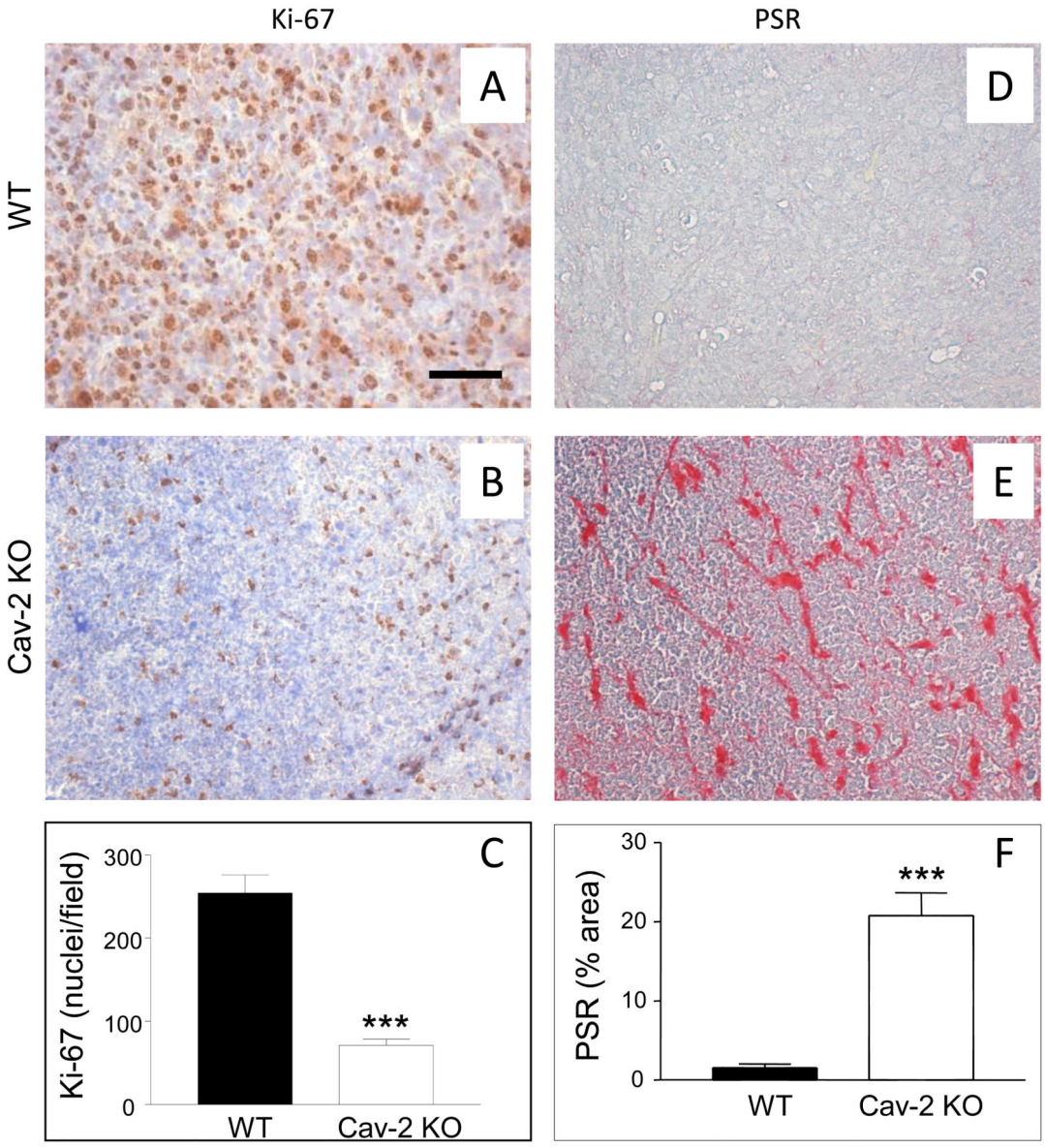

Figure 3. Cell proliferation and fibrosis within LLC tumors implanted into WT versus Cav-2 KO mice

5-um paraffin sections of the tumor tissue extracted 10 days after s.c. implantation of LLC cells into WT and Cav-2 KO mice were immunohistochemically stained with anti-Ki-67 antibody to label proliferative nuclei (AB) or histochemically stained with picrosirius red (PSR) to label extracellular collagen as an indicator of fibrosis (DE). C: Graphical representation of the average number of Ki-67-positive nuclei per field ± S.E.M. calculated from the total of 6-7 fields derived from two sections per group. ***, $P<0.0001$ compared with WT by unpaired t-test (n=7 for WT and n=6 for Cav-2 KO). F: Graphical representation of fibrosis quantified based on PSR staining from 8 fields derived from two section per group and expressed as mean percent area ± S.E.M. ***, $P<0.0001$ compared with WT by unpaired t-test (n=8 for WT and Cav-2 KO). Bar: 50 um.

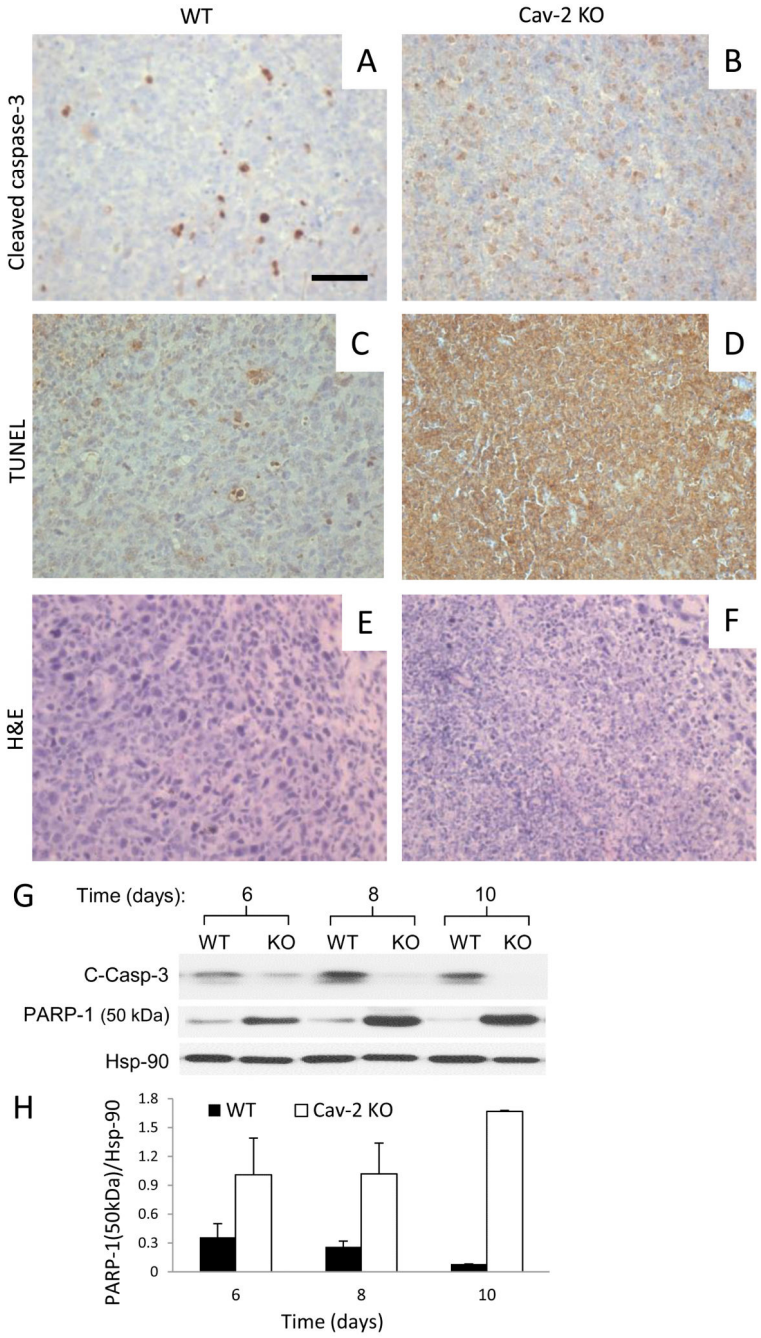

Figure 4. Cell death within LLC tumors implanted into WT versus Cav-2 KO mice

A-F: 5-um paraffin sections from LLC tumors extracted on day 10 after s.c. implantation were immunohistochemically stained with anti-cleaved caspase-3 antibody (AB), subjected to TUNEL staining (CD) or histochemically stained with H&E (EF). Bar: 50 um. G: Immunoblotting of LLC tumor lysates with antibodies against apoptotic cleaved caspase-3 (C-Casp-3), 50 kDa necrotic cleavage fragment of PARP-1 and Hsp-90. H: Quantitative densitometric ratio of 50 kDa necrotic cleavage fragment of PARP-1 (PARP-1 (50 kDa))/

Hsp-90 calculated based on immunoblots shown in G and expressed as mean ± S.D. from two replications based on one representative out of two total experiments.

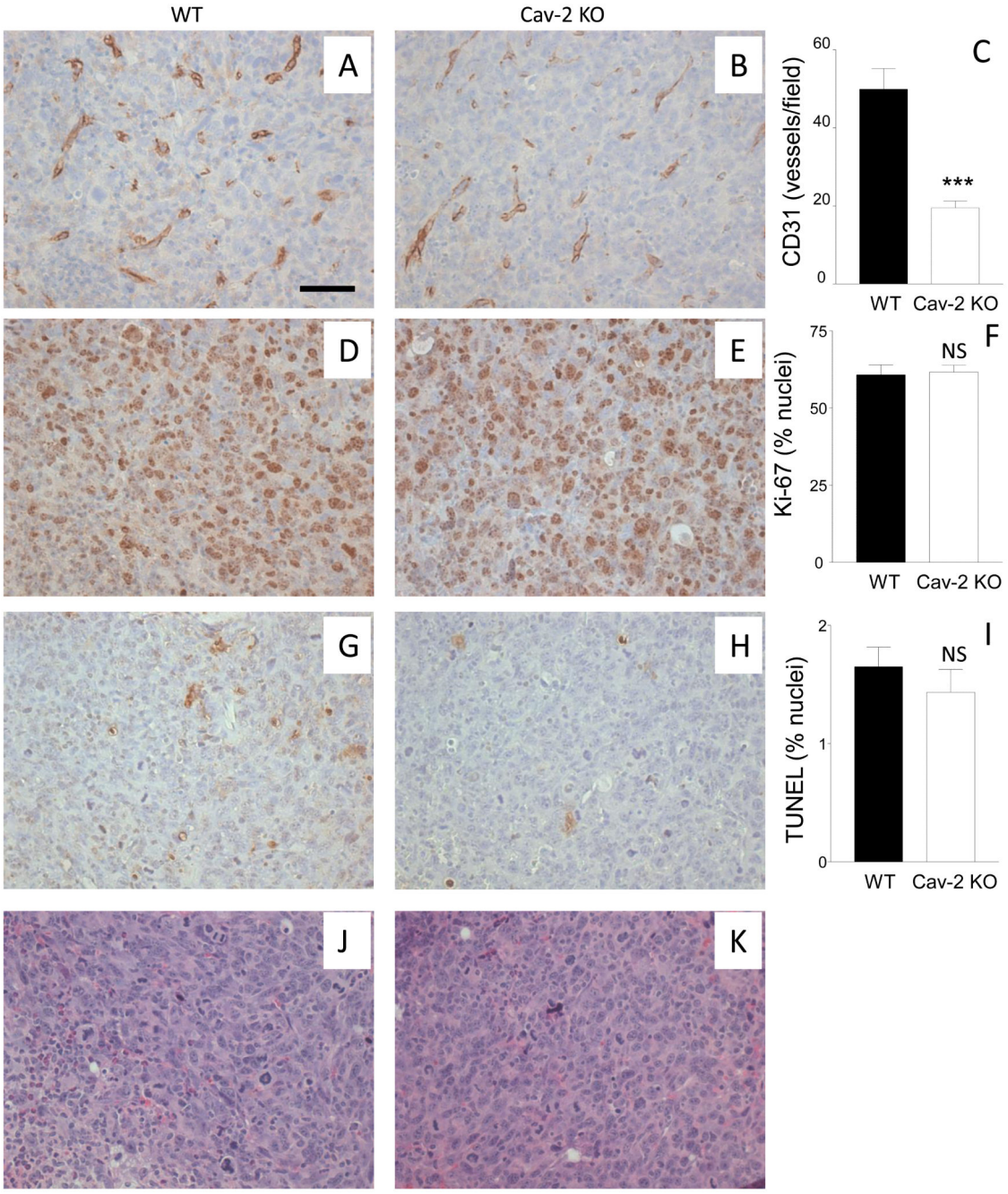

Figure 5. MVD versus cellular proliferation and death within the earliest palpable tumors extracted on day 6

5-um paraffin sections from earliest palpable tumors extracted 6 days after s.c. implantation of LLC cells were immunohistochemically stained with antibodies against CD31 (A,B) and Ki67 (D,E), TUNEL kit (G,H) or histochemically stained with H&E (J,K) to assess MVD, proliferation, apoptotic/non-apoptotic death, and gross cellular morphology, respectively, C: Graphical representation of MVD within the tumors quantified based on CD31 positive staining with the data expressed as mean numbers of CD31 positive vessels per field ± S.E.M. ***, P<0.0001 compared with WT by unpaired t-test (n=7 for WT and n=14 for

Cav-2 KO). F: Graphical representation of cell proliferation within tumors quantified based on Ki67 positive staining with the data expressed as mean numbers of Ki67 positive nuclei per field ± S.E.M. I: Graphical representation of cell death within tumors quantified based on TUNEL positive staining, with the data expressed as mean numbers of TUNEL positive nuclei per field ± S.E.M. NS, not statistically significant compared with WT by unpaired t-test (n=6 for WT for Cav-2 KO). Bar: 50 um.

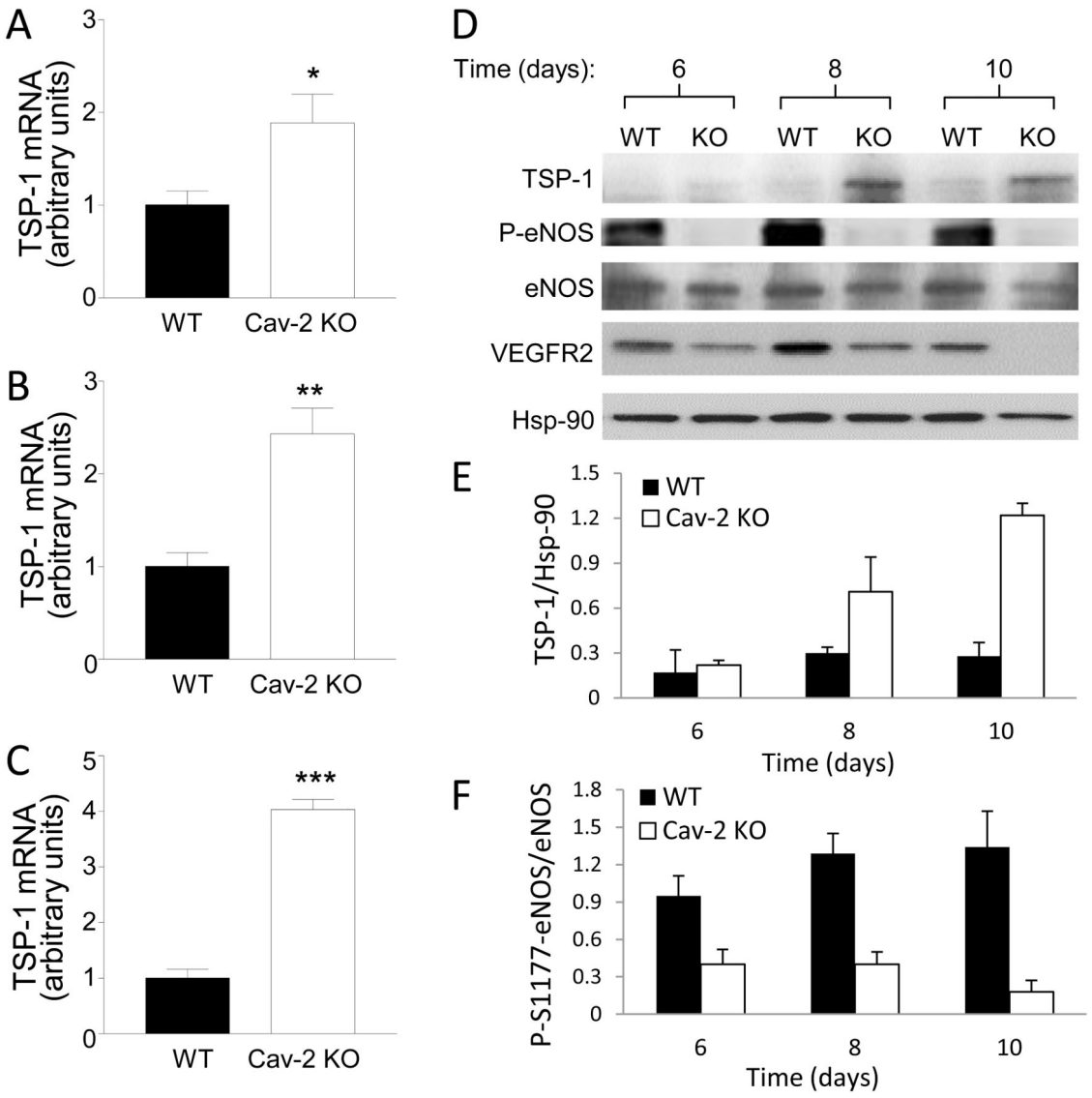

Figure 6. Molecular mechanisms associated with defective LLC tumor growth and angiogenesis in Cav-2 KO mice

A-C: qRT-PCR of TSP-1 mRNA extracted from LLC tumors 6 (A), 8 (B) and 10 (C) days after implantation. Values are calculated based on the amount of target mRNA normalized to the endogenous reference 18S rRNA mRNA. Data are expressed as mean ± SEM of 3 samples in 2 replications from one representative out of 3 total experiments. *, $P < 0.05$, **, $P<0.01$, and ***, $P<0.001$ compared with WT by unpaired t-test (n = 6). D: Immunoblotting of LLC tumor lysates with indicated antibodies against TSP-1, phospho-S1177-eNOS (P-eNOS), eNOS and Hsp-90. E-F: Quantitative densitometric ratios of TSP-1/Hsp-90 (E) and P-S1177-eNOS (P-eNOS)/eNOS (F) calculated based on immunoblots shown in D and expressed as mean ± S.D. from two replications based on one representative out of two total experiments.